



HAL
open science

Stereodivergent synthesis of chiral succinimides via Rh-catalyzed asymmetric transfer hydrogenation

Fangyuan Wang, Zongpeng Zhang, Yu Chen, Virginie Ratovelomanana-Vidal,
Peiyuan Yu, Gen-Qiang Chen, Xumu Zhang

► **To cite this version:**

Fangyuan Wang, Zongpeng Zhang, Yu Chen, Virginie Ratovelomanana-Vidal, Peiyuan Yu, et al..
Stereodivergent synthesis of chiral succinimides via Rh-catalyzed asymmetric transfer hydrogenation.
Nature Communications, 2022, 13 (1), pp.7794. 10.1038/s41467-022-35124-5 . hal-04270063

HAL Id: hal-04270063

<https://hal.science/hal-04270063v1>

Submitted on 6 Nov 2023

HAL is a multi-disciplinary open access archive for the deposit and dissemination of scientific research documents, whether they are published or not. The documents may come from teaching and research institutions in France or abroad, or from public or private research centers.

L'archive ouverte pluridisciplinaire **HAL**, est destinée au dépôt et à la diffusion de documents scientifiques de niveau recherche, publiés ou non, émanant des établissements d'enseignement et de recherche français ou étrangers, des laboratoires publics ou privés.

Stereodivergent synthesis of chiral succinimides via Rh-catalyzed asymmetric transfer hydrogenation

Received: 20 April 2022

Accepted: 18 November 2022

Published online: 17 December 2022

Check for updates

Fangyuan Wang^{1,4}, Zongpeng Zhang^{1,4}, Yu Chen^{1,4},
Virginie Ratovelomanana-Vidal², Peiyuan Yu¹✉, Gen-Qiang Chen³✉ &
Xumu Zhang¹✉

Chiral succinimide moieties are ubiquitous in biologically active natural products and pharmaceuticals. Until today, despite the great interest, little success has been made for stereodivergent synthesis of chiral succinimides. Here, we report a general and efficient method for accessing 3,4-disubstituted succinimides through a dynamic kinetic resolution strategy based on asymmetric transfer hydrogenation. The Rh catalyst system exhibit high activities, enantioselectivities, and diastereoselectivities (up to 2000 TON, up to >99% ee, and up to >99:1 dr). Products with *syn*- and *anti*-configuration are obtained separately by control of the reaction conditions. For the *N*-unprotected substrates, both the enol and the imide group can be reduced by control of reaction time and catalyst loading. In addition, the detailed reaction pathway and origin of stereoselectivity are elucidated by control experiments and theoretical calculations. This study offers a straightforward and stereodivergent approach to the valuable enantioenriched succinimides (all 4 stereoisomers) from cheap chemical feedstocks in a single reaction step.

Chiral 3-substituted and 3,4-disubstituted succinimide substructures are widely found in natural products and pharmaceuticals (Fig. 1)^{1–6}. Succinimide derivatives such as phensuximide (PTS), methsuximide (MTS) and ethosuximide (ETS), are well-known antiepileptic drugs (AEDs). In recent years, chiral succinimides have received great attention from synthetic chemists due to their wide range of biological activities such as antibacterial⁷, antifungal⁸, analgesic⁹, anticonvulsant¹⁰, and antitumor effects^{11,12}. The most well-developed methods include enantioselective cycloaddition reactions^{13–15} and hydrogenation reaction^{16–18} using maleimides as the substrates. Asymmetric catalytic addition^{19,20} of nucleophilic reagents to maleimides has also been reported (Fig. 2a). However, compared with well-developed synthetic methods of 3-substituted succinimides, few methodologies exist concerning the synthesis of 3,4-disubstituted succinimides^{19,21}.

The synthon, 3-hydroxy-4-substituted-succinimides can be easily converted to valuable chiral skeletons, such as chiral pyrrolidones and chiral lactams (Fig. 2c). Consequently, developing an efficient synthetic methodology for the construction of 3-hydroxy-4-substituted-succinimides from readily available starting materials is highly desirable.

Since the first asymmetric transfer hydrogenation (ATH) of ketones reported by Noyori and Ikariya using (*S,S*)-**cat.1**²², a series of catalysts containing *N*-monotosylated 1,2-diphenylethylenediamine (TsDPEN) have been documented by Noyori²², Ikariya²³, Wills^{24–26} and others^{27–42}. In 1999, Baiker et al. reported an enantioselective hydrogenation of pyrrolidine-2,3,5-triones using Pt–cinchonidine systems, obtaining 3,4-disubstituted succinimides with a single stereocenter¹⁶. Inspired by this work, we envisioned that 3-hydroxy-4-substituted maleimides could be reduced through a

¹Department of Chemistry, Shenzhen Grubbs Institute and Guangdong Provincial Key Laboratory of Catalysis, Southern University of Science and Technology, Shenzhen 518000, China. ²PSL University, Chimie ParisTech, CNRS, Institut1 of Chemistry for Life and Health Sciences, CSB2D team, 75005 Paris, France. ³Academy for Advanced Interdisciplinary Studies, Southern University of Science and Technology, Shenzhen 518000, China. ⁴These authors contributed equally: Fangyuan Wang, Zongpeng Zhang, Yu Chen. ✉e-mail: yupy@sustech.edu.cn; chengq@sustech.edu.cn; zhangxm@sustech.edu.cn

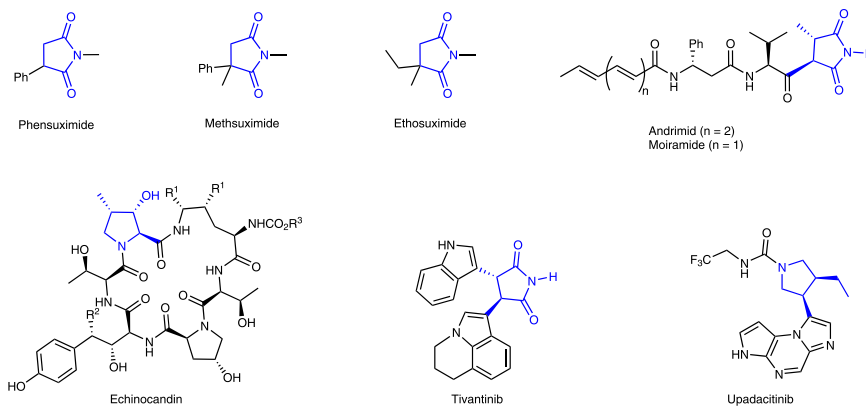


Fig. 1 | Biologically active compounds and drugs derived from succinimides. Phensuximide, methsuximide and ethosuximide are well-known antiepileptic drugs. Upadacitinib is a drug for the treatment of immune disorders, Echinocandins

have antifungal activities, and Tivantinib is used for the treatment of advanced hepatocellular carcinoma.

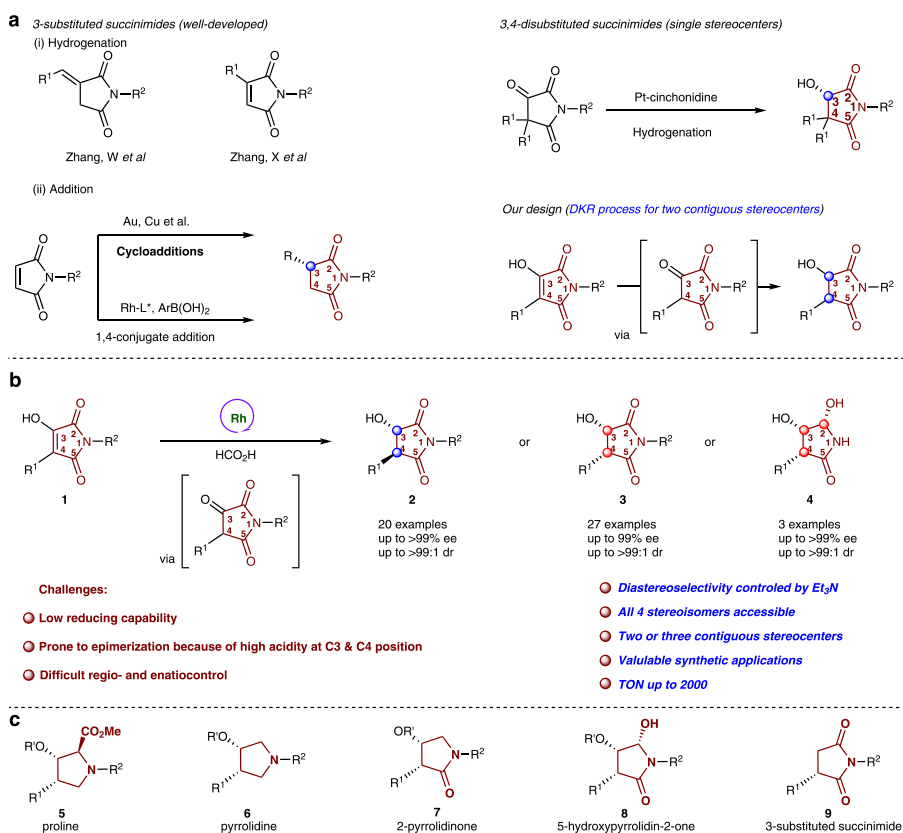
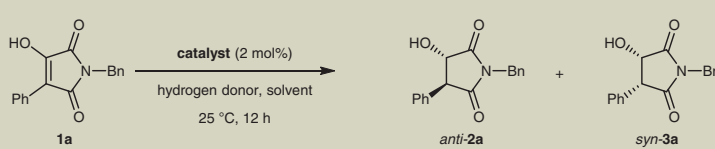


Fig. 2 | Synthetic methods for the construction of chiral succinimide derivatives. **a** Catalytic asymmetric synthesis of chiral succinimides (previous work). **b** Stereodivergent synthesis of chiral succinimide derivatives via ATH (this work). **c** Obtained building blocks.

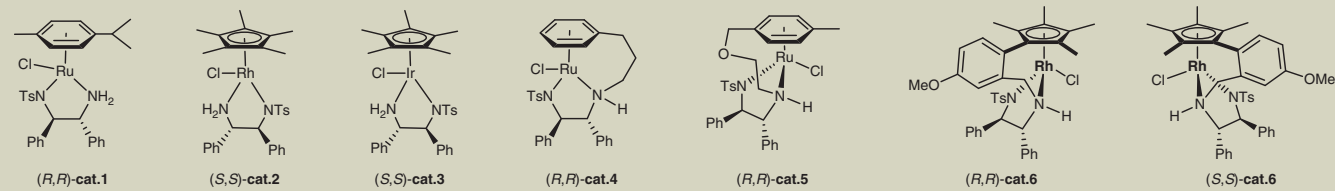
DKR (dynamic kinetic resolution)-ATH process. Over the past decades, DKR-ATH is an extremely attractive approach for the reduction of α -functional ketones due to the assured enantiomeric purity^{43–51}. In particular, base is necessary to facilitate the ATH process^{52,53}. Compared with well-studied α -functional ketones, 3-hydroxy-4-substituted maleimide (**1**) exists mainly in its enol form⁴⁵, and has low reducing activity under alkaline conditions. It can be reduced through the Pd/C-H₂ system but cannot be reduced by NaBH₄/MeOH system (for details, see Supplementary Fig. 9). Moreover, the corresponding reduction products are prone to epimerization under alkaline conditions. This also made it difficult to obtain the reduction

products using traditional alkaline reduction systems. Therefore, the development of appropriate asymmetric reduction methods to solve such problems is of great significance.

Herein, we report the stereodivergent enantio- and diastereoselective ATH of maleimide derivatives catalyzed by a tethered rhodium catalyst. Anti-3-hydroxy-4-substituted-succinimides **2** (up to >99% ee, up to >99:1 dr) and *syn*-3-hydroxy-4-substituted-succinimides **3** can be obtained by adjusting the amount of base (up to >99% ee, up to >99:1 dr). In addition, both the enol and the adjacent imide can be reduced to obtain **4** with high chemoselectivity by control the loading of the catalyst (up to >99% ee, up to >99:1 dr) (Fig. 2b).

Table 1 | Optimization for Rh(III)-catalyzed DKR-ATH of **1a^a**


Reaction scheme: Substrate **1a** (a chiral amide with a phenyl group and a hydroxyl group) reacts with a catalyst (2 mol%), hydrogen donor, and solvent at 25 °C for 12 h to yield *anti*-**2a** and *syn*-**3a**.



Chemical structures of catalysts: (R,R)-cat.1, (S,S)-cat.2, (S,S)-cat.3, (R,R)-cat.4, (R,R)-cat.5, (R,R)-cat.6, and (S,S)-cat.6.

entry	catalyst	Hydrogen donor	Solvent	conv. (%)	ee _{anti} (%)	ee _{syn} (%)	dr (<i>anti</i> / <i>syn</i>)
1	(R,R)-cat.1	HCO ₂ H:Et ₃ N (5:2)	MeOH	<5	–	–	–
2	(S,S)-cat.2	HCO ₂ H:Et ₃ N (5:2)	MeOH	<5	–	–	–
3	(S,S)-cat.3	HCO ₂ H:Et ₃ N (5:2)	MeOH	23	84	–	84:16
4	(R,R)-cat.4	HCO ₂ H:Et ₃ N (5:2)	MeOH	99	–96	–	90:10
5	(R,R)-cat.5	HCO ₂ H:Et ₃ N (5:2)	MeOH	90	–95	–	92:8
6	(R,R)-cat.6	HCO ₂ H:Et ₃ N (5:2)	MeOH	84	–96	–	95:5
7	(S,S)-cat.6	HCO ₂ H:Et ₃ N (5:2)	MeOH	85	96	–	95:5
8	(S,S)-cat.6	HCO ₂ H:Et ₃ N (5:2)	hexane	<5	–	–	–
9	(S,S)-cat.6	HCO ₂ H:Et ₃ N (5:2)	EtOH	71	93	–	97:3
10	(S,S)-cat.6	HCO ₂ H:Et ₃ N (5:2)	DCM	66	95	–	93:7
11	(S,S)-cat.6	HCO ₂ H:Et ₃ N (5:2)	THF	81	99	–	96:4
12	(S,S)-cat.6	HCO ₂ H:Et ₃ N (5:2)	dioxane	97	99	–	93:7
13	(S,S)-cat.6	HCO ₂ H:Et ₃ N (5:2)	toluene	>99	95	–	98:2
14	(S,S)-cat.6	HCO ₂ H:Et ₃ N (5:2)	EtOAc	>99	99	–	98:2
15 ^b	(S,S)-cat.6	HCO ₂ H:Et ₃ N (2:0.02)	EtOAc	>99	–	96	2:98
16 ^c	(S,S)-cat.6	HCO ₂ H:Et ₃ N (2:0)	EtOAc	>99	–	93	<1:99
17 ^d	(S,S)-cat.6	ⁱ PrOH	ⁱ PrOH	<5	–	–	–
18 ^e	(S,S)-cat.6	HCO ₂ Na	ⁱ PrOH	<5	–	–	–

^aConditions: Catalyst/**1a** (0.1 mmol) ratio of 1:50 in 1 mL of solvent, HCO₂H/Et₃N azeotropic mixture (20 μ L) at 25 °C for 12 h. Conversions (conv.) were determined by ¹H NMR analysis. Enantiomeric excesses (ee) and diastereomeric ratios (dr) were determined by HPLC analysis using a chiral stationary phase.

^bHCO₂H (2.0 equiv.) was used.

^cHCO₂H (2.0 equiv.) was used for 48 h.

^dKO^tBu (3.0 equiv.) was used in 1.0 mL of ⁱPrOH at 60 °C for 12 h.

^eHCO₂Na (5.0 equiv.) was used in 2.0 mL of ⁱPrOH /H₂O (1.0 mL/1.0 mL) at 60 °C for 12 h.

Results

Condition optimization

To investigate the proposed ATH process, model substrate **1a** was subjected to reduction using the commercially available TsDPEN-derived Ru, Rh and Ir complexes (2 mol%) in an azeotropic mixture of formic acid and triethylamine at 25 °C in MeOH. (Table 1) The Noyori's catalyst (R,R)-cat.1 and (S,S)-cat.2 cannot achieve any catalytic conversion (entries 1–2). Ir complexes, (S,S)-cat.3 can only achieve 23% conversion with 84% ee and 84:16 dr (entry 3). In contrast, the tethered-catalysts, cat.4–cat.5 showed more excellent conversion, enantioselectivity and diastereoselectivity. 96% ee and 90:10 dr were achieved with (R,R)-cat.4 while 95% ee and 92:8 dr were achieved with catalyst (R,R)-cat.5 (entries 4–5). To our great delight, the catalytic selectivity of Rh catalyst (R,R)-cat.6 and (S,S)-cat.6 outperformed that of the catalysts previously evaluated, providing corresponding product **2a** with 95:5 dr and 96% ee in an *anti*-selective manner (entries 6–7). (S,S)-cat.6 proved to be potential catalysts for the DKR-ATH of **1a**.

With (S,S)-cat.6 as a catalyst, we further explored the effects of solvents and the ratio of formic acid and triethylamine (Table 1). Several solvents, such as EtOH, DCM, THF, dioxane, toluene, hexane and EtOAc were examined with HCO₂H/Et₃N (5:2) for 12 h (entries 8–14). Except for

a low conversion in hexane (<5% conv.), moderate to high conversion and high stereoselectivity were observed in other solvents. Pleasingly, when EtOAc was used, excellent enantioselectivity and diastereoselectivity were obtained in full conversion (entry 14, 99% ee, 98:2 dr). On the contrary, *syn*-product **3a** was obtained by reducing the amount of trimethylamine (entry 15). When only formic acid was used, the enantioselectivity of the product decreased slightly, and extended reaction time was necessary to achieve full conversion (entry 16). In addition, different ratios of triethylamine and formic acid were investigated in EtOAc (Supplementary Table 1 presents details), indicating that the decrease in the proportion of Et₃N resulted in a decrease in the proportion of *anti*-product. Finally, isopropanol and sodium formate were also investigated as hydrogen donors, and a very low reactivity was observed under the alkaline environment (entries 17–18, <5% conv.). So far, HCO₂H/Et₃N (5:2) was used as a hydrogen donor for *anti*-**2a** (entry 14) and HCO₂H/Et₃N (2.0 equiv./0.02 equiv.) for *syn*-**3a** (entry 15).

Substrate scope

Under the optimal conditions, the methodology using of HCO₂H/Et₃N (5:2) as a hydrogen source was successfully extended to a series of substrates, and the results were illustrated in Fig. 3. Substrates with the

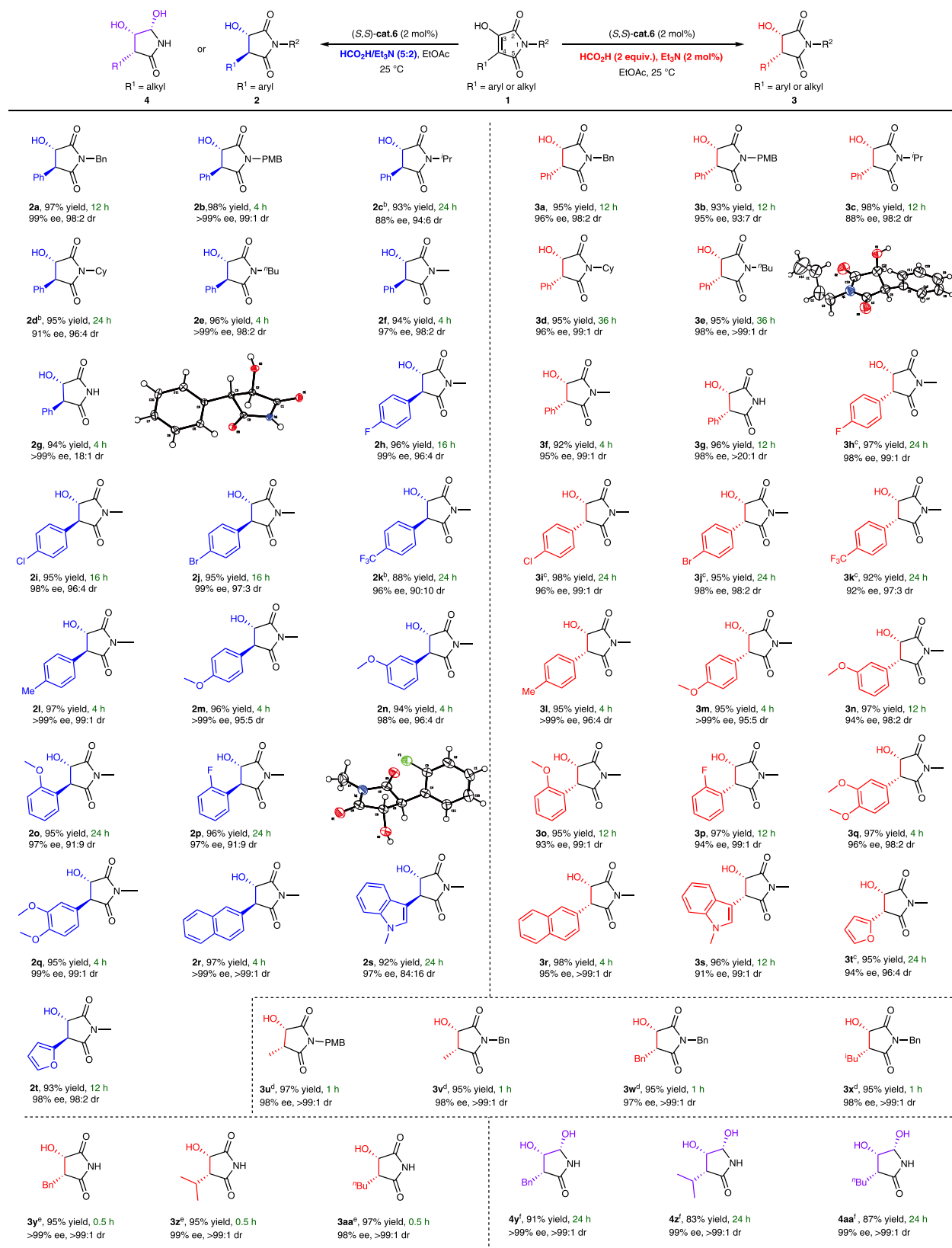


Fig. 3 | Substrate scope. ^aConducted with catalyst/substrate (0.2 mmol) ratio of 1: 50 in 1 mL of solvent, HCO₂H (2.0 equiv.)/Et₃N (2 mol%) for *syn*-isomer **3** and HCO₂H/Et₃N azeotropic mixture (20 μL) were used for 1 h. ^c(S,S)-cat.6 (1 mol%) and HCO₂H/Et₃N azeotropic mixture (20 μL) were used for 1 h. ^d(S,S)-cat.6 (1 mol%) and HCO₂H/Et₃N azeotropic mixture (20 μL) were used for 0.5 h. ^e(S,S)-cat.6 (5 mol%) and HCO₂H/Et₃N azeotropic mixture (40 μL) were used for 24 h.

and HCO₂H/Et₃N azeotropic mixture (50 μL) were used. ^c(S,S)-cat.6 (5 mol%) and HCO₂H (2.0 equiv.) and HCO₂H/Et₃N azeotropic mixture (20 μL) were used for 1 h. ^d(S,S)-cat.6 (1 mol%) and HCO₂H/Et₃N azeotropic mixture (20 μL) were used for 1 h. ^e(S,S)-cat.6 (1 mol%) and HCO₂H/Et₃N azeotropic mixture (20 μL) were used for 0.5 h. ^f(S,S)-cat.6 (5 mol%) and HCO₂H/Et₃N azeotropic mixture (40 μL) were used for 24 h.

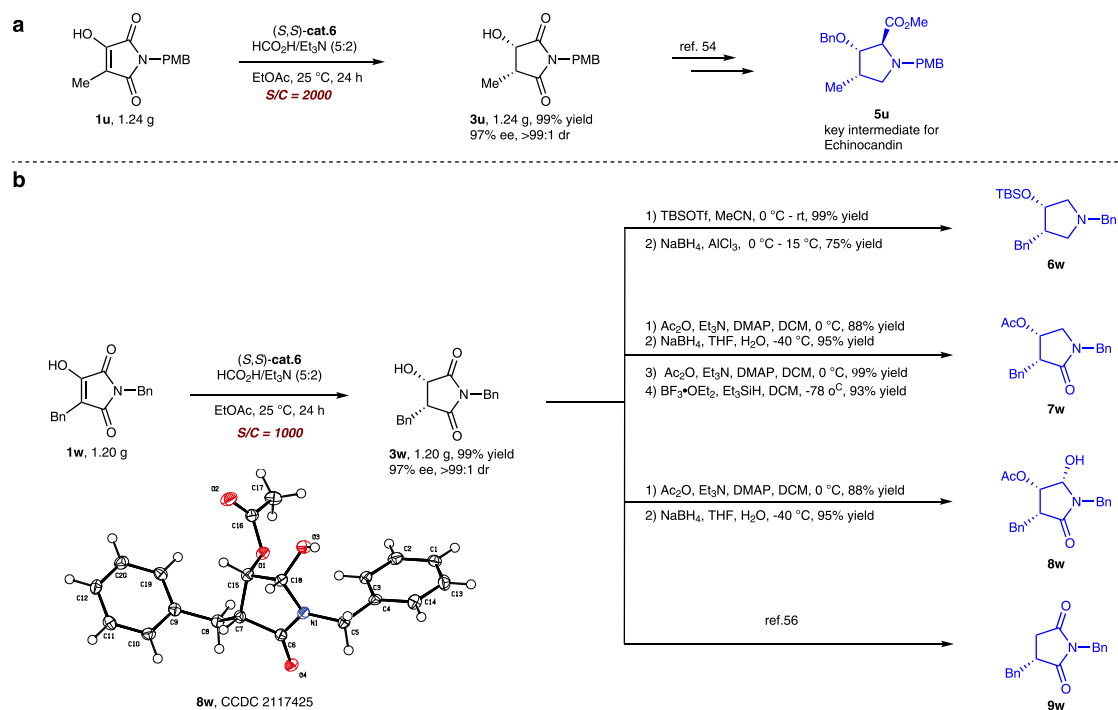


Fig. 4 | Gram scale synthetic utilities of the DKR-ATH process. a Gram-scale experiment of **1u**. **b** Gram-scale experiment of **1w** and transformations of product **3w**.

different protective groups on the nitrogen atom were subjected to the standard reaction conditions, and the reaction proceeded smoothly to provide the *anti*-product with high yields, excellent enantioselectivities and diastereoselectivities (**2a–2g**, 94–98% yield, 94:6–>99:1 dr, 88%–>99% ee). Next, we evaluated the effect of the substituents on the C4 position. Functional groups, such as halides (**2h–2j**), trifluoromethyl (**2k**), methyl (**2l**), methoxy (**2m**) at the *para* position of the phenyl group were compatible with this transformation (88–97% yield, 90:10–99:1 dr, 96%–>99% ee). Substrates with *meta*-substitution on the phenyl group were also tolerated, and 98% ee and 96:4 dr were obtained (**2n**). In addition, the *ortho*-methoxy and *ortho*-fluoro substrate were evaluated with lower dr values (**2o–2p**, 95–96% yield, 91:9 dr and 97% ee). Moreover, the product **2r** with 3,4-methoxy groups on the phenyl ring was obtained with 99% ee and 99:1 dr. The current reaction also tolerates substrates bearing 2-naphthyl, 2-furanyl, and 3-indolyl groups (**2r–2t**, 92%–95% yield, 84:16–99:1 dr, 97–99% ee).

Subsequently, a sharp contrast was exhibited using HCO₂H (2.0 equiv.)/Et₃N (2 mol%) as a hydrogen source, and the *syn*-products could be obtained selectively. (Fig. 3) High enantioselectivities and diastereoselectivities were obtained with a wide range of *N*-protected substrates (**3a–3g**, 93–98% yield, 93:7–>99:1 dr, 88–98% ee). The effect of substitution at the C4 position of the substrates was also evaluated, and products with halides, trifluoromethyl, methyl, and methoxy group at the *ortho*, *meta*, or *para* position of the phenyl group were smoothly produced in 92–98% yields with 95:5–99:1 dr and up to >99% ee (**3h–3q**). 2-Naphthyl-containing substrates could obtain excellent enantioselectivity and diastereoselectivity as well (**3r**, 98% yield, >99:1 dr, 98% ee). Heterocycle-containing substrates, such as indole (**3s**, 91% ee, 99:1 dr) and furan (**3t**, 94% ee, 96:4 dr) were compatible with the conditions. For substrates with alkyl substitution at the C4 position, using an azeotropic mixture of HCO₂H/Et₃N (5:2) as a hydrogen source, this transformation proceeded smoothly to provide the *syn*-product in excellent yields (up to 97%) and with high levels of diastereo- and enantioselectivities (**3u–3x**, 97–98% ee, >99:1 dr). What's more, *N*-unprotected substrates were well tolerated (**3y–3aa**, 98%–>99% ee, >99:1 dr). Interestingly, for *N*-unprotected substrates, both the enol

and imide groups can be reduced. The products 4,5-dihydroxy-3-alkylpyrrolidin-2-one, containing three contiguous stereocenters, can be obtained by increasing the loading of catalyst (**4y–4aa**, 98%–>99% ee, >99:1 dr).

Synthetic applications

To demonstrate the synthetic utilities of this methodology, two gram-scale transformations were conducted, and the results were summarized in Fig. 4. To our delight, when 0.05 mol% (S/C = 2000) catalyst loading was used, the gram-scale experiment proceeded smoothly to provide **3u** with excellent results. According to the procedure in the literature, **3u** can be further transformed into the important synthon **5u** (3-hydroxy-4-methylproline), which is a key intermediate for Echinocandin (Fig. 4a)⁵⁴. Similarly, the ATH of **1w** could be performed with a catalyst loading of 0.1 mol% to obtain **3w** with excellent results. Then it can be further transformed into pyrrolidine derivative **6w**, lactam derivatives **7w**⁵⁵, **8w**, and succinimide derivative **9w**⁵⁶ in high yield and excellent stereoselectivity (Fig. 4b).

Mechanism study

To elucidate the detailed mechanism of this ATH process, a series of mechanistic investigations were conducted, and the results were summarized in Fig. 5. First, the reaction of hydroxyl-protected substrate **1a'** was conducted under the standard conditions, and **2a'** was obtained with only 37–38% ee and 85/15-87/13 dr, which means that the presence of the –OH group at the C3-position is necessary to ensure high enantioselectivity, and the C=C reduction pathway is also possible. (Fig. 5a). Second, the *syn*-product **3a** can be smoothly transformed into the *anti*-product **2a** in the presence of an azeotropic mixture of HCO₂H/Et₃N (5:2). This suggested that the *anti*-product was probably produced by epimerization of the *syn*-product. Interestingly, **3y** can be transformed into the **4y** with three contiguous stereocenters (Fig. 5b). Moreover, the reaction kinetic experiment showed that **1a** can be completely reduced in preference to **1a'** under standard conditions (Fig. 5c). During the process, the reduction of **1a** first produced the *syn*-product which isomerized to the *anti*-product along with the process of the reaction, whereas, the reduction of **1a'** obtained the

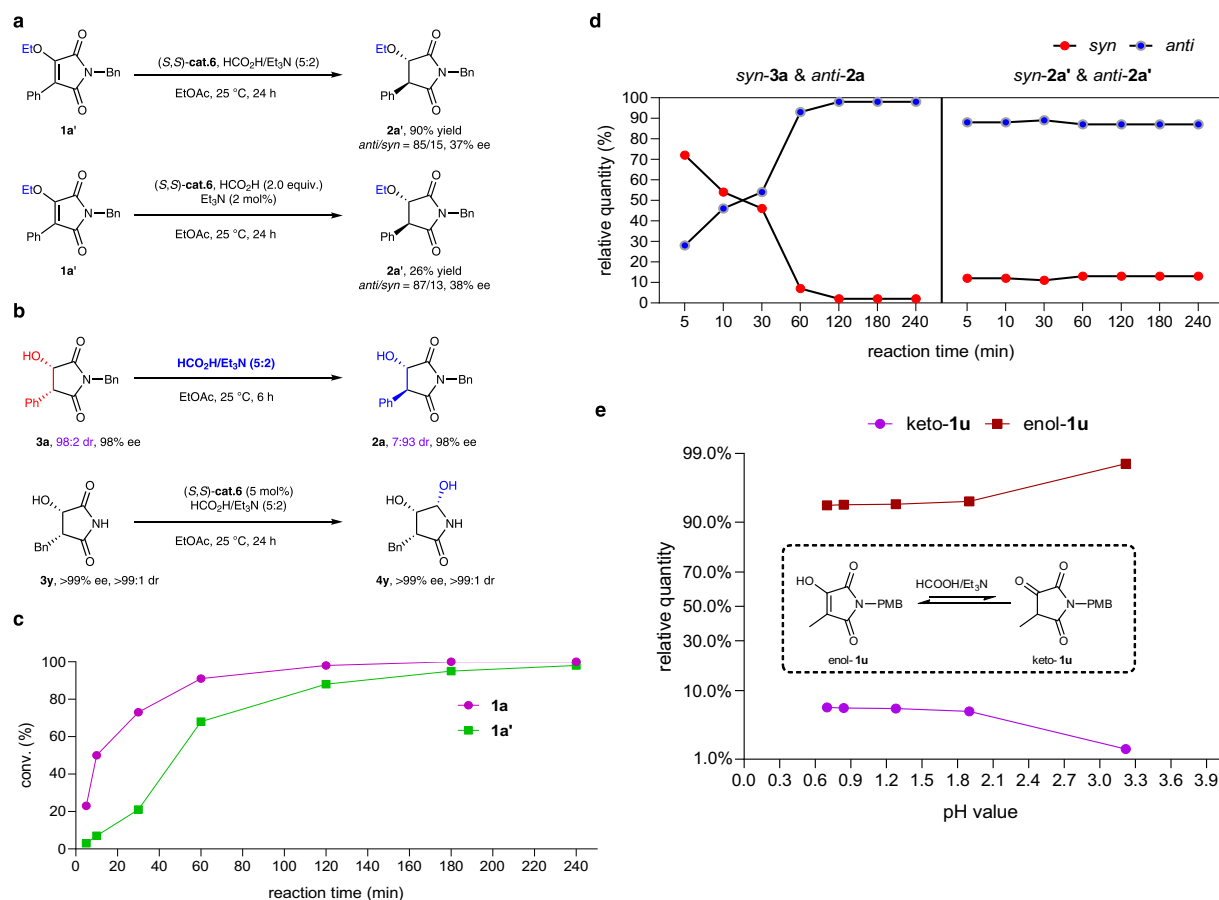


Fig. 5 | Mechanistic investigations. **a** Reactions of ethyl-protected substrate under standard conditions. **b** Observed effect of HCO₂H/Et₃N (5:2) on the diastereoselectivities. **c** Kinetic experiments of **1a** and **1a'**. **d** Monitoring of the reaction

process of **1a** and **1a'** under standard conditions. **e** Effect of pH on the relative quantity of enol and keto form of **1u**.

anti-product mainly, and the *anti/syn* ratio changed slightly during the reaction process (Fig. 5d). In addition, the keto-enol equilibrium experiment revealed that the ratio of enol-**1u** increased with the increase of pH value in acidic environment (Fig. 5e). Our mechanistic investigations revealed that the current reaction probably proceeded via reduction of the keto form.

The mechanistic investigations and theoretical data^{57,58} accumulated for the ATH of **1** point to two plausible catalytic cycles. Key results from DFT calculations, including the most favorable reaction pathways for C=O and C=C reduction, respectively, are shown in Fig. 6. Active catalyst **cat1** was generated from decarboxylation of the formate complex of **cat.6** (Supplementary Fig. 11 and Supplementary Data 1). In the catalytic cycle for C=O reduction, **cat1** interacts with substrate keto-**1g** to generate the intermediate **a-R-int1**, followed by a direct hydride (H⁻) transfer via transition state **a-RS-TS1**, with an energy barrier of 3.1 kcal/mol relative to **a-R-int1**. This step generates an intermediate **a-RS-int2**, which is more stable than **a-R-int1** by 11.3 kcal/mol. Subsequently, the proton transfer step is completed via **a-RS-TS2** by overcoming the energy barrier of 12.9 kcal/mol relative to **a-RS-int2**. The active catalyst **cat1** is regenerated after releasing of the *syn*-product **RS-pro** followed by proton transfer from formic acid. Finally, considering that active catalyst **cat1** first more easily capture enol-**1g** than keto-**1g** to form a more stable intermediate **int1** in an exergonic process of 2.6 kcal/mol, the free energy barrier of the C=O reduction pathway from **cat1** to product should be 15.0 kcal/mol from **int1** to **a-RS-TS1**. On the other hand, for the catalytic cycle of the C=C reduction, the hydride transfer step suffered from an energy barrier of 19.7 kcal/mol via transition state **S-TS1** relative to **int1**. The following proton

transfer step has an energy barrier of 21.1 kcal/mol relative to **int1**. Subsequent release of the *anti*-product **SS-pro** and interaction with formic acid regenerates **cat1** and produces CO₂. The results show that from **cat1**, the free energy barrier of the most favorable pathway for C=O and C=C reduction are respectively 15.0 kcal/mol (from **int1** to **a-RS-TS1**) and 21.1 kcal/mol (from **int1** to **SS-TS2**), and are consistent with the experimental observation that the formation of the *anti*-product is favored over the *syn*-product. The CO₂ generated in the asymmetric reduction with formic acid can be effectively removed from the catalytic system. In addition, the theoretical study of the C=C reduction pathway for the hydroxyl-protected substrate was also conducted under standard conditions (Supplementary Fig. 12 and Supplementary Data 1 present the details).

The free energies and key lengths of the transition states leading to different stereoselective products were also shown in Fig. 7. For the C=O reduction pathway, it is found that the transition state **a-RS-TS1** has a significant advantage relative to other three transition states **a-SS-TS1**, **a-SR-TS1**, and **a-RR-TS1** by 6.2, 7.5, and 10.8 kcal/mol, respectively. The proton transfer step in the C=C reduction pathway is the enantio/rate-determining step, the transition state **SS-TS2** is more stable than the other three transition states **RS-TS2**, **SR-TS2**, and **RR-TS2** by 9.2, 12.7, and 2.6 kcal/mol, respectively. Comparing to the reduction of the C=C, **a-RS-TS1** is more favorable than the corresponding transition states **SS-TS2** by 6.1 kcal/mol. The result showed that reduction of the C=O bond is the more reasonable pathway, resulting in the formation of *syn*-product, which can transform into the *anti*-product in the presence of Et₃N. The reduction of the C=C path need to overcome a higher energy barrier (21.1 kcal/mol vs 15.0 kcal/mol) and form the *anti*-product in the

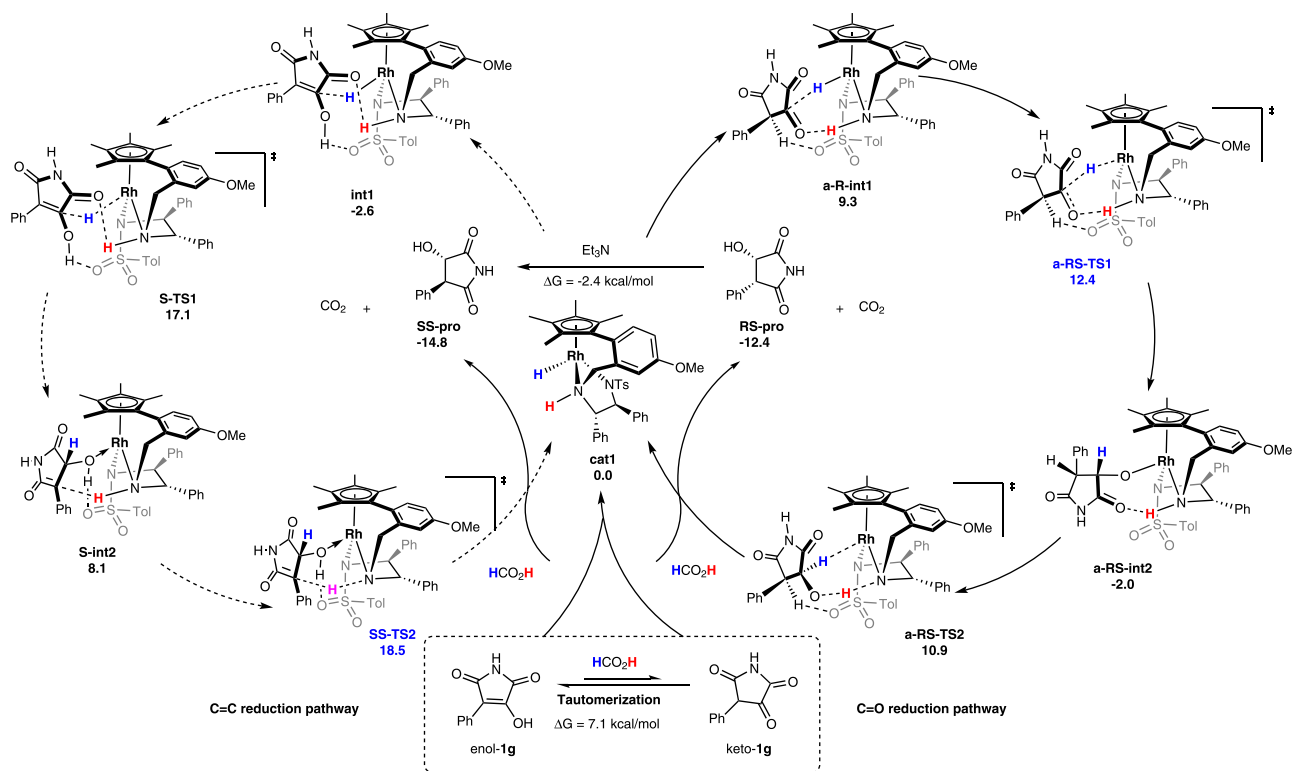


Fig. 6 | Proposal catalytic cycle for ATH of **1g** with **HCOOH**. The C=C reduction pathway was depicted in the left catalytic cycle and the C=O reduction pathway was described in the catalytic cycle on the right. The Gibbs free energy of the

compounds, intermediates and transition states are provided below the corresponding chemical structures and the energies are given in kcal/mol.

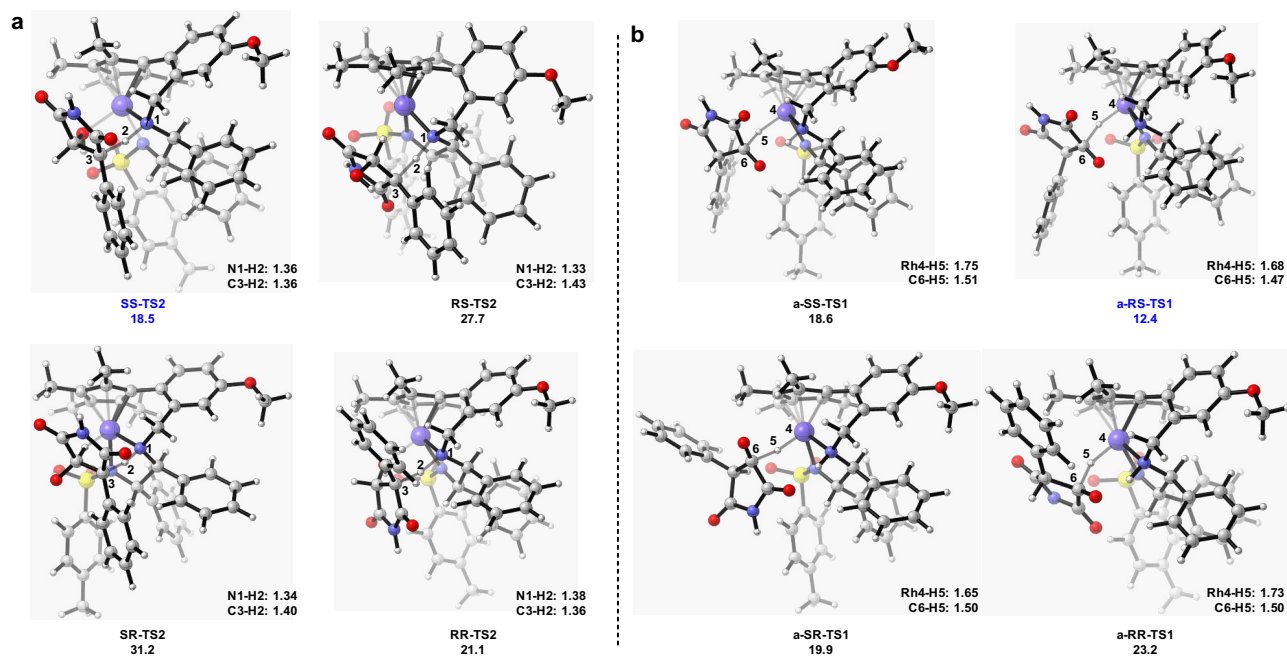


Fig. 7 | The free energies of the transition states of the enantio-determining steps. **a** Calculated transition states for the C=O bond reduction pathway. **b** Calculated transition states for the C=C bond reduction pathway. The energies are given in kcal/mol. The lengths are given in angstrom.

catalytic cycle, which is also inconsistent with the experimental results of the formation of *syn*-product.

Discussion

In conclusion, a highly asymmetric transfer hydrogenation of 3-hydroxy-4-substituted-maleimide derivatives was successfully developed using a

tethered Rh catalyst under mild reaction conditions. Through strategic modulation of the amount of Et_3N , a variety of 3-hydroxy-4-substituted-maleimide were transformed into the corresponding *syn*- and *anti*-chiral succinimides with excellent enantio- and diastereoselectivities. This method successfully breaks the inherent impression of single product in previously reported ATH methodologies. Comprehensive

mechanistic studies revealed that the -OH group at the C3-position of **1** is crucial for driving the reaction to the high enantioselectivity, and the configuration of the product will undergo epimerization during the ATH process. This also leads to two possible reduction processes (C=O or C=C). Computational analysis revealed that the C=C reduction pathway may suffer a higher energy barrier than the C=O reduction pathway, and it cannot generate the *syn*-product. Thus, the C=O reduction pathway via dynamic kinetics resolution process is reasonable. In addition, gram-scale experiments and varieties of transformation at high TONs provides an efficient way to synthesis chiral pyrrolidine derivatives. The present findings demonstrate successful mechanistic control to realize the ATH of a challenging substrate, which can provide further insight into the development of ATH.

Methods

Representative procedure of asymmetric transfer hydrogenation of **1a**

To a 10 mL Schleck tube charged with a magnetic stirring bar were added successively substrate **1a** (0.2 mmol, 56 mg), formic acid/triethylamine azeotropic mixture (5/2) (40 μ L), **cat.6** (3 mg, 0.004 mmol) and the solvent (2 mL). The mixture was then stirred at room temperature for the indicated reaction time. After completion, the reaction solution was concentrated and the residue was passed through a short column of silica gel (eluent: EtOAc:PE = 2:1) to produce **2a** as a white solid (55 mg, 97% yield, 99% ee, 98:2 dr). The ee or dr values of compound **2a** were determined by HPLC analysis on a chiral stationary phase (Chiralpak IE column, hexane/isopropanol = 80/20; flow rate = 1.0 mL/min; UV detection at 210 nm; t_1 = 8.9 min, t_2 = 9.9 min, t_3 = 10.6 min, t_4 = 13.4 min (major).

Data availability

The authors declare that the data supporting the findings of this study are available within the paper and its supplementary information files. Crystallographic data for compounds **2g**, **2p**, **3e**, **8w** have been deposited in the Cambridge Structural Database with the deposition numbers 2040537, 2074951, 2074952, and 2117425 respectively. Copies of the crystallographic data can be obtained free of charge via <https://www.ccdc.cam.ac.uk/structures/>.

References

1. Needham, J., Kelly, M. T., Ishige, M. & Andersen, R. J. Andrimid and moiramides A-C, metabolites produced in culture by a marine isolate of the bacterium *Pseudomonas fluorescens*: structure elucidation and biosynthesis. *J. Org. Chem.* **59**, 2058–2063 (2002).
2. Mohapatra, D. K., Mondal, D., Chorghade, M. S. & Gurjar, M. K. General strategy for a short and efficient synthesis of 3-hydroxy-4-methylprolines (HMP). *Tetrahedron Lett.* **47**, 9215–9219 (2006).
3. Nguyen, H. T. et al. In vitro and in vivo antibacterial activity of serratamid, a novel peptide-polyketide antibiotic isolated from *Serratia plymuthica* C1, against phytopathogenic bacteria. *J. Agric. Food Chem.* **69**, 5471–5480 (2021).
4. Ohashi, M. et al. Biosynthesis of para-cyclophane-containing hirsutellone family of fungal natural products. *J. Am. Chem. Soc.* **143**, 5605–5609 (2021).
5. Taylor, J. G. et al. Discovery of the pan-genotypic hepatitis C virus NS3/4A protease inhibitor voxilaprevir (GS-9857): A component of Vosevi(R). *Bioorg. Med. Chem. Lett.* **29**, 2428–2436 (2019).
6. Remsing Rix, L. L. et al. GSK3 α and β are new functionally relevant targets of tivantinib in lung cancer cells. *ACS Chem. Biol.* **9**, 353–358 (2014).
7. Pohlmann, J. et al. Pyrrolidinedione derivatives as antibacterial agents with a novel mode of action. *Bioorg. Med. Chem. Lett.* **15**, 1189–1192 (2005).
8. Fujinami, A., Ozaki, T., Nodera, K. & Tanaka, K. Studies on biological activity of cyclic imide compounds: Part II. Antimicrobial activity of l-phenylpyrrolidine-2,5-diones and related compounds. *Agric. Biol. Chem.* **36**, 318–323 (1972).
9. Obniska, J. et al. Antinociceptive properties of N-Mannich bases derived from 3-substituted pyrrolidine-2,5-dione in the formalin model of persistent pain in mice. *Pharmacol. Rep.* **67**, 63–68 (2015).
10. Rapacz, A. et al. Evaluation of anticonvulsant and antinociceptive properties of new N-Mannich bases derived from pyrrolidine-2,5-dione and 3-methylpyrrolidine-2,5-dione. *Naunyn-Schmiedeberg's Arch. Pharm.* **389**, 339–348 (2016).
11. Okino, T., Qi, S., Matsuda, H., Murakami, M. & Yamaguchi, K. Nosotapeptins A and B, elastase inhibitors from the cyanobacterium *Nostoc minutum*. *J. Nat. Prod.* **60**, 158–161 (1997).
12. Zhao, Z. et al. Research progress in biological activities of succinimide derivatives. *Bioorg. Chem.* **108**, 104557 (2021).
13. Ghannay, S. et al. Stereoselective synthesis of enantiopure N-substituted pyrrolidin-2,5-dione derivatives by 1,3-dipolar cycloaddition and assessment of their in vitro antioxidant and antibacterial activities. *Bioorg. Med. Chem. Lett.* **27**, 2302–2307 (2017).
14. Hashimoto, T. & Maruoka, K. Recent advances of catalytic asymmetric 1,3-dipolar cycloadditions. *Chem. Rev.* **115**, 5366–5412 (2015).
15. Melhado, A. D., Luparia, M. & Toste, F. D. Au(I)-catalyzed enantioselective 1,3-dipolar cycloadditions of α -methylacrylates with electron-deficient alkenes. *J. Am. Chem. Soc.* **129**, 12638–12639 (2007).
16. Szabo, A., Künzle, N., Mallat, T. & Baiker, A. Enantioselective hydrogenation of pyrrolidine-2,3,5-triones over the Pt-cinchonidine system. *Tetrahedron: Asymmetry* **10**, 61–76 (1999).
17. Han, Z. et al. Highly enantioselective synthesis of chiral succinimides via Rh/bisphosphine-thiourea-catalyzed asymmetric hydrogenation. *ACS Catal.* **6**, 6214–6218 (2016).
18. Liu, Y. & Zhang, W. Iridium-catalyzed asymmetric hydrogenation of α -alkylidene succinimides. *Angew. Chem. Int. Ed.* **52**, 2203–2206 (2013).
19. Shintani, R., Duan, W. L. & Hayashi, T. Rhodium-catalyzed asymmetric construction of quaternary carbon stereocenters: ligand-dependent regiocontrol in the 1,4-addition to substituted malimides. *J. Am. Chem. Soc.* **128**, 5628–5629 (2006).
20. Duan, W. L., Iwamura, H., Shintani, R. & Hayashi, T. Chiral phosphine-olefin ligands in the rhodium-catalyzed asymmetric 1,4-addition reactions. *J. Am. Chem. Soc.* **129**, 2130–2138 (2007).
21. Sakkani, N. & Nanda, S. K. A review on the synthesis and applications of α -alkylidene succinimides. *Asian J. Org. Chem.* <https://doi.org/10.1002/ajoc.202200041> (2022).
22. Fujii, A., Hashiguchi, S., Uematsu, N., Ikariya, T. & Noyori, R. Ruthenium(II)-catalyzed asymmetric transfer hydrogenation of ketones using a formic acid-triethylamine mixture. *J. Am. Chem. Soc.* **118**, 2521–2522 (1996).
23. Touge, T. et al. Oxo-tethered ruthenium(II) complex as a bifunctional catalyst for asymmetric transfer hydrogenation and H₂ hydrogenation. *J. Am. Chem. Soc.* **133**, 14960–14963 (2011).
24. Matharu, D. S., Morris, D. J., Kawamoto, A. M., Clarkson, G. J. & Wills, M. A stereochemically well-defined rhodium(III) catalyst for asymmetric transfer hydrogenation of ketones. *Org. Lett.* **7**, 5489–5491 (2005).
25. Vyas, V. K., Clarkson, G. J. & Wills, M. Sulfone group as a versatile and removable directing group for asymmetric transfer hydrogenation of ketones. *Angew. Chem. Int. Ed.* **59**, 14265–14269 (2020).
26. Vyas, V. K., Clarkson, G. J. & Wills, M. Enantioselective synthesis of bicyclopentane-containing alcohols via asymmetric transfer hydrogenation. *Org. Lett.* **23**, 3179–3183 (2021).

27. Zhang, J., Blazecka, P. G., Bruendl, M. M. & Huang, Y. Ru-TsDPEN with formic acid/Hunig's base for asymmetric transfer hydrogenation, a practical synthesis of optically enriched N-propyl pantolactam. *J. Org. Chem.* **74**, 1411–1414 (2009).
28. Steward, K. M., Corbett, M. T., Goodman, C. G. & Johnson, J. S. Asymmetric synthesis of diverse glycolic acid scaffolds via dynamic kinetic resolution of α -keto esters. *J. Am. Chem. Soc.* **134**, 20197–20206 (2012).
29. Steward, K. M., Gentry, E. C. & Johnson, J. S. Dynamic kinetic resolution of α -keto esters via asymmetric transfer hydrogenation. *J. Am. Chem. Soc.* **134**, 7329–7332 (2012).
30. Echeverria, P.-G., Féraud, C., Phansavath, P. & Ratovelomanana-Vidal, V. Synthesis, characterization and use of a new tethered Rh(III) complex in asymmetric transfer hydrogenation of ketones. *Catal. Commun.* **62**, 95–99 (2015).
31. Krabbe, S. W. & Johnson, J. S. Asymmetric total syntheses of megacerotonic acid and shimobashiric acid. *Org. Lett.* **17**, 1188–1191 (2015).
32. Cotman, A. E., Cahard, D. & Mohar, B. Stereoarrayed CF₃-substituted 1,3-diols by dynamic kinetic resolution: ruthenium(II)-catalyzed asymmetric transfer hydrogenation. *Angew. Chem. Int. Ed.* **55**, 5294–5298 (2016).
33. Fang, L., Liu, S., Han, L., Li, H. & Zhao, F. Ruthenium-catalyzed synthesis of cis-2,3-dihydrobenzofuran-3-ols by aqueous transfer hydrogenation via dynamic kinetic resolution. *Organometallics* **36**, 1217–1219 (2017).
34. Jeran, M., Cotman, A. E., Stephan, M. & Mohar, B. Stereopure functionalized benzosultams via ruthenium(II)-catalyzed dynamic kinetic resolution-asymmetric transfer hydrogenation. *Org. Lett.* **19**, 2042–2045 (2017).
35. Sun, G. et al. Highly enantioselective synthesis of syn- β -hydroxy α -dibenzylamino esters via DKR asymmetric transfer hydrogenation and gram-scale preparation of droxidopa. *Org. Lett.* **19**, 4339–4342 (2017).
36. Zheng, D. et al. A dynamic kinetic asymmetric transfer hydrogenation-cyclization tandem reaction: an easy access to chiral 3,4-dihydro-2H-pyran-carbonitriles. *Chem. Commun.* **53**, 6113–6116 (2017).
37. Cotman, A. E., Lozinsek, M., Wang, B., Stephan, M. & Mohar, B. trans-Diastereoselective Ru(II)-catalyzed asymmetric transfer hydrogenation of α -acetamido benzocyclic ketones via dynamic kinetic resolution. *Org. Lett.* **21**, 3644–3648 (2019).
38. Molina Betancourt, R., Phansavath, P. & Ratovelomanana-Vidal, V. Rhodium-catalyzed asymmetric transfer hydrogenation/dynamic kinetic resolution of 3-benzylidene-chromanones. *Org. Lett.* **23**, 1621–1625 (2021).
39. Zheng, L. S., Féraud, C., Phansavath, P. & Ratovelomanana-Vidal, V. Rhodium-mediated asymmetric transfer hydrogenation: a diastereo- and enantioselective synthesis of syn- α -amido β -hydroxy esters. *Chem. Commun.* **54**, 283–286 (2018).
40. Touge, T. et al. Multiple absolute stereocontrol in cascade lactone formation via dynamic kinetic resolution driven by the asymmetric transfer hydrogenation of keto acids with Oxo-tethered ruthenium catalysts. *J. Am. Chem. Soc.* **141**, 16354–16361 (2019).
41. Luo, Z. et al. η^6 -Arene CH–O interaction directed dynamic kinetic resolution—asymmetric transfer hydrogenation (DKR-ATH) of α -keto/enol-lactams. *Adv. Synth. Catal.* **363**, 3030–3034 (2021).
42. Touge, T., Nara, H., Kida, M., Matsumura, K. & Kayaki, Y. Convincing catalytic performance of Oxo-tethered ruthenium complexes for asymmetric transfer hydrogenation of cyclic α -halogenated ketones through dynamic kinetic resolution. *Org. Lett.* **23**, 3070–3075 (2021).
43. Wang, D. & Astruc, D. The golden age of transfer hydrogenation. *Chem. Rev.* **115**, 6621–6686 (2015).
44. Ratovelomanana-Vidal, V., Phansavath, P., Echeverria, P.-G. & Ayad, T. Recent developments in asymmetric hydrogenation and transfer hydrogenation of ketones and imines through dynamic kinetic resolution. *Synthesis* **48**, 2523–2539 (2016).
45. Bhat, V., Welin, E. R., Guo, X. & Stoltz, B. M. Advances in stereoconvergent catalysis from 2005 to 2015: transition-metal-mediated stereoablative reactions, dynamic kinetic resolutions, and dynamic kinetic asymmetric transformations. *Chem. Rev.* **117**, 4528–4561 (2017).
46. Seo, C. S. G. & Morris, R. H. Catalytic homogeneous asymmetric hydrogenation: successes and opportunities. *Organometallics* **38**, 47–65 (2018).
47. Zhang, Y., Zhang, Y. & Ramstrom, O. Dynamic covalent kinetic resolution. *Cat. Rev. Sci. Eng.* **62**, 66–95 (2020).
48. Cotman, A. E. Escaping from flatland: stereoconvergent synthesis of three-dimensional scaffolds via ruthenium(II)-catalyzed Noyori-Ikariya transfer hydrogenation. *Chem. Eur. J.* **27**, 39–53 (2021).
49. Luo, Z. et al. Ruthenium-catalyzed highly enantioselective synthesis of cis-3-quinuclidinols via DKR asymmetric transfer hydrogenation. *Org. Lett.* **22**, 4322–4326 (2020).
50. Talavera, G., Santana Farina, A., Zanotti-Gerosa, A. & Nedden, H. G. Structural diversity in ruthenium-catalyzed asymmetric transfer hydrogenation reactions. *Top. Organomet. Chem.* **65**, 73–114 (2019).
51. Molina Betancourt, R., Echeverria, P.-G., Ayad, T., Phansavath, P. & Ratovelomanana-Vidal, V. Recent progress and applications of transition-metal-catalyzed asymmetric hydrogenation and transfer hydrogenation of ketones and imines through dynamic kinetic resolution. *Synthesis* **53**, 30–50 (2021).
52. Kim, H. R., Achary, R. & Lee, H. K. DBU-promoted dynamic kinetic resolution in Rh-catalyzed asymmetric transfer hydrogenation of 5-Alkyl cyclic sulfamidate imines: stereoselective synthesis of functionalized 1,2-amino alcohols. *J. Org. Chem.* **83**, 11987–11999 (2018).
53. He, B., Phansavath, P. & Ratovelomanana-Vidal, V. Kinetic resolution of 2-aryl-2,3-dihydroquinolin-4(1H)-one derivatives by rhodium-catalyzed asymmetric transfer hydrogenation. *Org. Chem. Front.* **8**, 2504–2509 (2021).
54. Meng, W.-H., Wu, T.-J., Zhang, H.-K. & Huang, P.-Q. Asymmetric syntheses of protected (2S,3S,4S)-3-hydroxy-4-methylproline and 4'-tert-butoxyamido-2'-deoxythymidine. *Tetrahedron.: Asymmetry* **15**, 3899–3910 (2004).
55. Hwang, D. J., Kim, S. N., Choi, J. H. & Lee, Y. S. Dicafeoyl- or digalloyl pyrrolidine and furan derivatives as HIV integrase inhibitors. *Bioorg. Med. Chem.* **9**, 1429–1437 (2001).
56. Lin, G.-J., Luo, S.-P., Zheng, X., Ye, J.-L. & Huang, P.-Q. Enantiodivergent synthesis of trans-3,4-disubstituted succinimides by SmI₂-mediated Reformatsky-type reaction. *Tetrahedron Lett.* **49**, 4007–4010 (2008).
57. Dub, P. A. & Gordon, J. C. Metal-ligand bifunctional catalysis: The “Accepted” mechanism, the issue of concertedness, and the function of the ligand in catalytic cycles involving hydrogen atoms. *ACS Catal.* **7**, 6635–6655 (2017).
58. Dub, P. A. et al. Enantioselectivity in the Noyori-Ikariya asymmetric transfer hydrogenation of ketones. *Organometallics* **40**, 1402–1410 (2021).

Acknowledgements

X.Z. is indebted to National Key R&D Program of China (2021YFA1500201), Shenzhen Nobel Prize Scientists Laboratory Project (C17213101), Key-Area Research and Development Program of Guangdong Province (No. 2020B010188001), Guangdong Provincial Key Laboratory of Catalysis (No. 2020B121201002), Innovative Team of Universities in Guangdong Province (No. 2020KCXTD016), and National Natural Science Foundation of China (No. 21991113). G.-Q. Chen

gratefully acknowledges the National Natural Science Foundation of China (Nos. 21901107, 22171129), the Guangdong Basic and Applied Basic Research Foundation (No. 2022B1515020055) and the Shenzhen Science and Technology Innovation Committee (No. JCYJ20210324104202007) for financial support. Computational work was supported by Center for Computational Science and Engineering at Southern University of Science and Technology, and the CHEM high-performance supercomputer cluster (CHEM-HPC) located at the Department of Chemistry, Southern University of Science and Technology. The authors acknowledge the assistance of SUSTech Core Research Facilities. This article is dedicated to professor J. P. Collman on the occasion of his 90th birthday.

Author contributions

F.W., Z.Z., and Y.C. contributed equally to this work. F.W. and Z.Z. contributed to the conception and design of the experiments. F.W. and Z.Z. performed the experiments and analyzed the data. Y.C. completed the DFT calculation. P.Y. directed the calculation section. V.R.-V. directed the synthesis of the catalyst. G.-Q.C. and X.Z. directed the project. F.W. and G.-Q.C. co-wrote the manuscript.

Competing interests

The authors declare no competing interests.

Additional information

Supplementary information The online version contains supplementary material available at <https://doi.org/10.1038/s41467-022-35124-5>.

Correspondence and requests for materials should be addressed to Peiyuan Yu, Gen-Qiang Chen or Xumu Zhang.

Peer review information *Nature Communications* thanks Eric R. Ashley, and the other, anonymous, reviewers for their contribution to the peer review of this work.

Reprints and permissions information is available at <http://www.nature.com/reprints>

Publisher's note Springer Nature remains neutral with regard to jurisdictional claims in published maps and institutional affiliations.

Open Access This article is licensed under a Creative Commons Attribution 4.0 International License, which permits use, sharing, adaptation, distribution and reproduction in any medium or format, as long as you give appropriate credit to the original author(s) and the source, provide a link to the Creative Commons license, and indicate if changes were made. The images or other third party material in this article are included in the article's Creative Commons license, unless indicated otherwise in a credit line to the material. If material is not included in the article's Creative Commons license and your intended use is not permitted by statutory regulation or exceeds the permitted use, you will need to obtain permission directly from the copyright holder. To view a copy of this license, visit <http://creativecommons.org/licenses/by/4.0/>.

© The Author(s) 2022